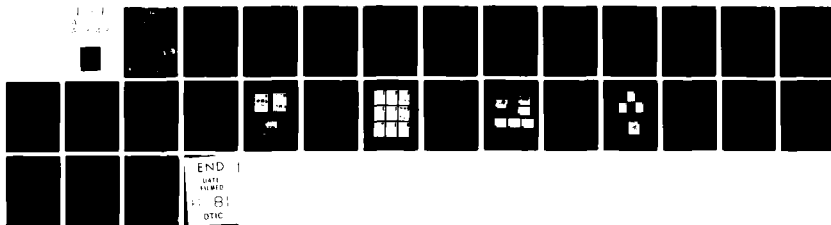
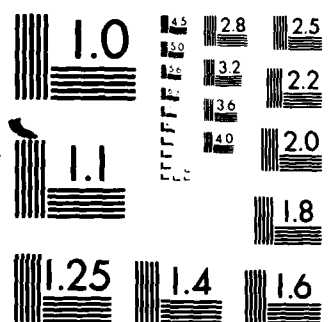


AD-A099 413

AEROSPACE CORP EL SEGUNDO CA CHEMISTRY AND PHYSICS LAB F/G 14/2
SCANNING AUGER AND WORK-FUNCTION MEASUREMENTS APPLIED TO DISPEN--ETC(U)
MAY 81 G ENG. H K KAN
TR-0081(6970-02)-1 SD-TR-81-35 F04701-80-C-0081
NL

UNCLASSIFIED





MICROCOPY RESOLUTION TEST CHART
NATIONAL BUREAU OF STANDARDS 1963-A

AD A099413

1 May 1968

Approved for Release by NSA on 05-11-2014 pursuant to E.O. 13526


Prepared for
SPACE DIVISION
AIR FORCE SYSTEMS COMMAND
Los Angeles Air Force Station
P.O. Box 92900, Worldway Postal Center
Los Angeles, Calif. 90009


81 5 28 012

This report was submitted by The Aerospace Corporation, El Segundo, CA 90245, under Contract No. F04701-80-C-0081 with the Space Division, Deputy for Technology, P.O. Box 92960, Worldway Postal Center, Los Angeles, CA 90009. It was reviewed and approved for The Aerospace Corporation by M. T. Weiss, Acting Director, Chemistry and Physics Laboratory. Lt Randall S. Weidenheimer, SD/YLVS, was the project officer for the Mission-Oriented Investigation and Experimentation (MOIE) Programs.


This report has been reviewed by the Public Affairs Office (PAS) and is releasable to the National Technical Information Service (NTIS). At NTIS, it will be available to the general public, including foreign nations.

This technical report has been reviewed and is approved for publication. Publication of this report does not constitute Air Force approval of the report's findings or conclusions. It is published only for the exchange and stimulation of ideas.


Randall S. Weidenheimer, 2nd Lt, USAF
Project Officer


Florian P. Meinhardt, Lt Col, USAF
Director of Advanced Space Development

FOR THE COMMANDER


William Goldberg, Colonel, USAF
Deputy for Technology

UNCLASSIFIED

SECURITY CLASSIFICATION OF THIS PAGE (When Data Entered)

9/73 final rept;

19 REPORT DOCUMENTATION PAGE		READ INSTRUCTIONS BEFORE COMPLETING FORM	
1. REPORT NUMBER SD-TR-81-35	2. GOVT ACCESSION NO. AD-A099	3. RECIPIENT'S CATALOG NUMBER 413	
4. TITLE (and Subtitle) SCANNING AUGER AND WORK-FUNCTION MEASUREMENTS APPLIED TO DISPENSER CATHODES		5. TYPE OF REPORT & PERIOD COVERED	
7. AUTHOR(s) Genghun / Eng H. K. Alan / Kan		6. PERFORMING ORG. REPORT NUMBER TR-0081(6970-02)-1	
		8. CONTRACT OR GRANT NUMBER(s) F04701-80-C-0081	
9. PERFORMING ORGANIZATION NAME AND ADDRESS The Aerospace Corporation El Segundo, Calif. 90245		10. PROGRAM ELEMENT, PROJECT, TASK AREA & WORK UNIT NUMBERS	
11. CONTROLLING OFFICE NAME AND ADDRESS Space Division Air Force Systems Command Los Angeles, Calif. 90009		12. REPORT DATE 1 May 81	
14. MONITORING AGENCY NAME & ADDRESS (if different from Controlling Office)		13. NUMBER OF PAGES 29	
		15. SECURITY CLASS. (of this report) Unclassified	
		15a. DECLASSIFICATION/DOWNGRADING SCHEDULE	
16. DISTRIBUTION STATEMENT (of this Report) Approved for public release; distribution unlimited			
17. DISTRIBUTION STATEMENT (of the abstract entered in Block 20, if different from Report)			
18. SUPPLEMENTARY NOTES			
19. KEY WORDS (Continue on reverse side if necessary and identify by block number) Auger Analysis Dispenser Cathodes Spatially Resolved Measurements Work Function			
20. ABSTRACT (Continue on reverse side if necessary and identify by block number) A method to perform spatially resolved work-function measurements has been developed using a modified scanning Auger microprobe (SAM). The basis of the method is that patches of different work function give rise to different onsets of secondary electron emission. The combined SAM-work function measurement method permits a microscopic correlation of emissive or surface dipole properties with elemental composition. The system permits a surface spatial resolution of 0.2 μm provided by the focused incident electron beam, and a work-function resolution of better than 0.05 eV. Results are presented for			

DD FORM 1473
(FACSIMILE)

409313

UNCLASSIFIED
SECURITY CLASSIFICATION OF THIS PAGE (When Data Entered)

UNCLASSIFIED

SECURITY CLASSIFICATION OF THIS PAGE(When Data Entered)

19. KEY WORDS (Continued)

20. ABSTRACT (Continued)

elemental samples, which were used as a test of the work-function mapping ability. Some initial results on dispenser cathode surfaces are also presented.

3

UNCLASSIFIED

SECURITY CLASSIFICATION OF THIS PAGE(When Data Entered)

PREFACE

We wish to thank G. W. Stupian and R. L. Corbin for their advice and assistance and P. W. Palmberg for useful suggestions. We would also like to thank G. A. Haas and R. E. Thomas for helpful discussions on their retarding-beam method.

Accession For	
NTIS GRA&I	<input checked="checked" type="checkbox"/>
DTIC TAB	<input type="checkbox"/>
Unannounced	<input type="checkbox"/>
Justification	
By	
Distribution/	
Availability Codes	
Dist	Avail and/or Special
A	

CONTENTS

PREFACE.....	1
I. INTRODUCTION.....	7
II. WORK-FUNCTION MEASUREMENT PRINCIPLE.....	9
III. EXPERIMENTAL CONFIGURATION.....	13
IV. RESULTS AND DISCUSSION.....	15
A. Results Using Element Samples.....	15
B. Results on Commercial Dispenser Cathodes.....	18
C. Comparison of Secondary Electron Onset Technique with a Retarding-Beam Method.....	22
D. Accuracy of Work-Function Determination.....	24
V. CONCLUSIONS.....	29

FIGURES

1.	Work-Function Differences Measured through Shifts in Onset of Secondary Electron Emission Spectrum.....	10
2.	Experimental Configuration, Revealing Cathode Sample, Biasing Grid, and Scanning Auger Microprobe Analyzer.....	14
3.	Measured Shifts in Secondary Emission Onset Giving Work-Function Differences; Nb-W-Pt(Rh) Sample.....	16
4.	Test of Work-Function (ϕ) Mapping with the Use of Pt/Nb Sample, Revealing Low ϕ Regions as Nb, High ϕ Regions as Pt.....	17
5.	Individual Work-Function Maps, Cleaned Pt/Nb Sample, 0.2 eV Intervals.....	19
6.	Work-Function Distribution $n(\phi)$ Derived from Previous Figure, Normalized to Account for Differing Pt and Nb Surface Areas.....	20
7.	Example of Auger Elemental Distribution Taken on a Commercial Dispenser Cathode Surface During Activation Procedure ($\sim 800^\circ\text{C}$), Followed by Work-Function Maps (Room Temperature).....	21
8.	Work Function Maps Associated with a Cathode Microregion, after ~ 150 hr Heating at 1050°C , Revealing ϕ Correlation with Various Surface Features.....	23
9.	Calculated Effects of Patch Fields on Work-Function Measurement.....	26

I. INTRODUCTION

The work function ϕ is the energy barrier that electrons in a solid must overcome to escape into a vacuum. For cathode devices, work function is both a measure of the surface dipole configuration and the emissivity of the cathode surface through the use of the Richardson-Dushman equation.¹ In this report, the development of a technique to perform spatially resolved ϕ measurements on dispenser cathodes by means of the scanning electron beam and cylindrical energy analyzer associated with a scanning Auger microprobe (SAM) is outlined.

¹W. Nottingham, Thermionic Emission, Report 321, MIT Research Laboratory of Electronic Technology, Cambridge, Mass. (1956).

II. WORK-FUNCTION MEASUREMENT PRINCIPLE

The method selected to perform work-function measurements is based on the shifts in the onset of secondary electron emission and has been used previously in conjunction with X-ray photoelectron spectroscopy (XPS) measurements.^{2,3} This method is more compatible with the existing SAM analyzer configuration than a retarding beam method.⁴ The present method is illustrated in Fig. 1, which reveals an idealized emitter surface with patches of different work functions ϕ_1 and ϕ_2 . At any point on the sample, the emitter work-function value ϕ_e represents the local barrier height that must be surmounted by electrons. An applied accelerating voltage V_o separates the emitter Fermi level E_F^e from the collector Fermi level E_F^c by an energy eV_o . Because an incident kilovolt electron beam impinges onto the surface, the emitter Fermi electron sea is disturbed from thermal equilibrium. As a result, electrons that have an energy higher than the local barrier can escape into the vacuum, resulting in a secondary electron emission spectrum that covers a broad range of energies. This resultant $N(E)$ versus E curve is schematically shown in Fig. 1c. In this curve, the onset of the secondary electron spectrum, i.e., the lowest kinetic energy electrons collected, has a very specific energy: collector kinetic energy minimum = $(\phi_e - \phi_c) + eV_o$, where ϕ_c is the collector work-function value. Thus, with distinct patches on the emitter, ϕ_1 and ϕ_2 , the secondary electron spectrum from these different spatial points will have distinctly different onsets separated by a $\Delta\phi = \phi_2 - \phi_1$. In this manner, the work function of an inhomogeneous surface can be mapped relative to any fixed reference value by the measurement of differences in the onset of the secondary electron emission spectrum.

An accelerating potential V_o , supplied by an external grid, shifts the entire secondary electron spectrum to a higher energy region in which the

²S. Evans, Chem. Phys. Lett. **23** (1), 134 (1973).

³P. Ascarelli and G. Missoni, J. Electron. Spectroscopy Related Phenom. **5**, 417 (1974).

⁴G. A. Haas and R. E. Thomas, Surf. Sci. **4** (1), 64 (1966).

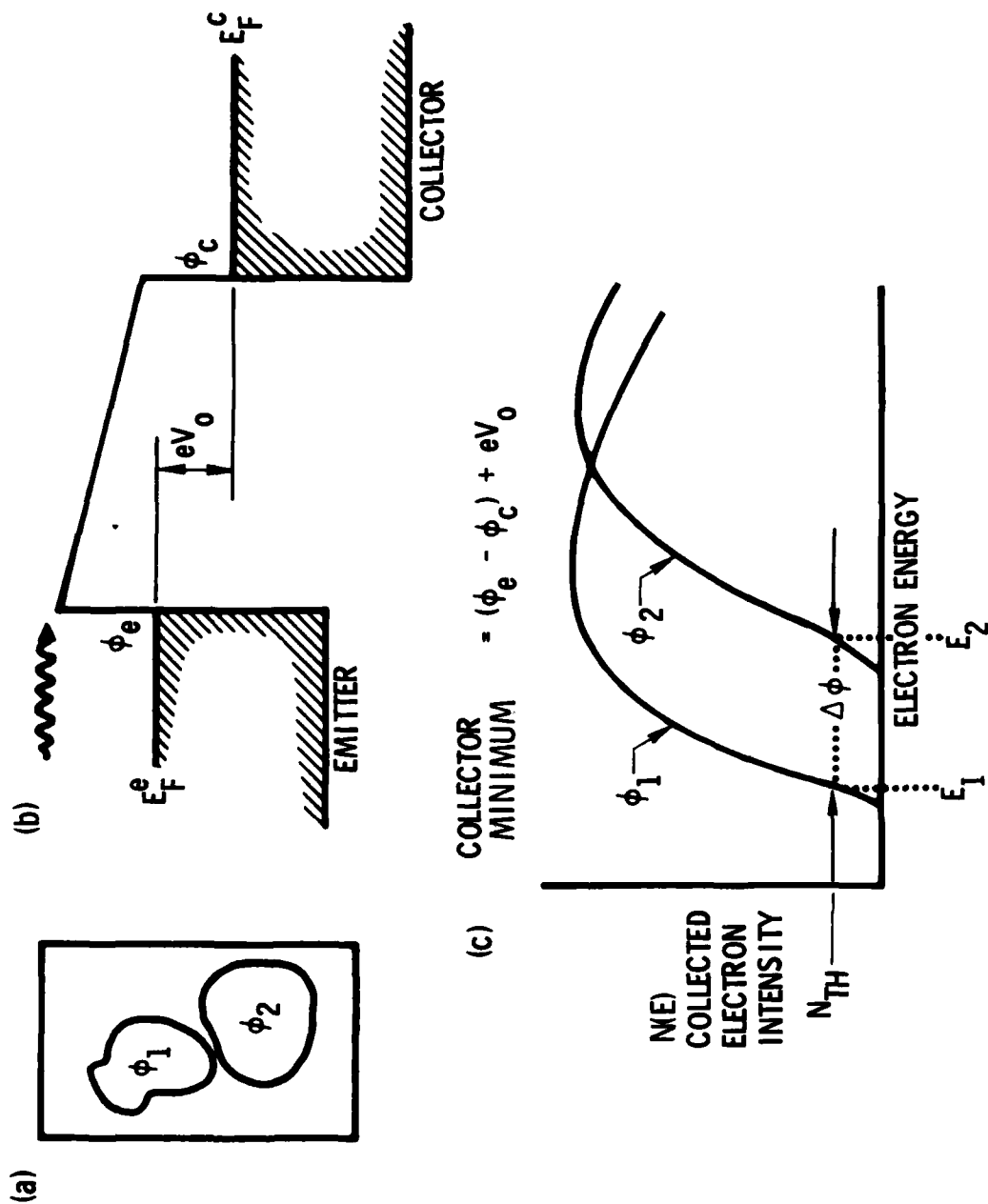


Fig. 1. Work-Function Differences Measured through Shifts in Onset of Secondary Electron Emission Spectrum

analyzer has a better gain performance. In addition, the high applied field reduces the effect of lateral patch fields associated with the surface ϕ differences. The work function is then determined with the use of a threshold level on the secondary electron spectrum labeled N_{th} , as illustrated in Fig. 1c. Theoretically, the onset should be very sharp,⁵ but measured signals characteristically show a sloping rise in the onset region, the slope being dependent on the electron excitation process in a given solid.⁶ However, if the threshold level N_{th} that is selected is low compared to the collected signal maximum, the work-function difference is then $\Delta\phi = e\Delta V$, where ΔV is the voltage difference between the two curves when $N(E) = N_{th}$.

For the production of a work-function map, the energy analyzer is set to scan within a given $\pm dE_1$ of a preset E_1 value. If the region addressed by the electron beam has a secondary electron emission spectrum which results in an $N(E)$ signal level that will coincide with the N_{th} level, a bright dot is recorded on a screen. Otherwise, the field remains dark, indicating surface regions with either higher or lower work function. A two-dimensional contour, which is a band $\pm dE_1$ about a fixed value of ϕ , is then mapped by this bright dot pattern. By changing the E_1 level to a new value E'_1 , a second contour band can be generated. The superposition of the set of contour bands, each representing a small $\pm dE_1$ about a given ϕ value, results in the total spatially resolved work-function distribution of the surface. Because these maps indicate only differences in work function, an absolute value can be obtained after calibration with a surface of known work function.

The primary limitation of the use of the secondary electron onset is that it cannot be used for samples where thermionic emission is large. Thus, for the examination of cathode surfaces, the temperature must be lowered so that the thermionic electron emission is small compared to the secondary electron emission caused by electron beam bombardment, because a large low-energy electron spike that overlaps the secondary emission onset would be introduced

⁵P. A. Wolff, Phys. Rev. **95** (1), 55 (1964).

⁶H. J. Fitting et al., Surf. Sci. **75** (2), 267 (1978).

by thermionic emission from a substrate. This signal can originate from any location on the sample surface and hence contains no spatially resolved information. Note, however, that Auger analyses are not affected because Auger electrons are characteristically higher in energy (greater than 25 eV) compared to thermionic electrons (less than 2 eV), and the Auger electrons can easily be distinguished from a large thermionic background by the analyzer. Consequently, for the examination of dispenser cathodes, in-situ Auger analyses were performed at high temperatures, followed by rapid cooling to freeze in the high-temperature surface elemental distribution, and work-function analyses were then subsequently performed at the lower temperature. Experience has revealed no change in the Auger spectrum upon cooling. Therefore, the chemical composition of the surface should remain unchanged, indicating that the ϕ measurement at lower temperatures may not be a serious limitation.

III. EXPERIMENTAL CONFIGURATION

A Physical Electronics Industries Model 590 scanning Auger microprobe (SAM) was used as the primary instrument. An electron beam of energy up to approximately 8 keV, which can be rastered and focused to 0.2 μm diameter, is provided by the SAM. The system has an energy analysis capability of 0 to 2000 eV and a useful magnification range of 20 to 5000X. The focus point for the analyzer is located so that electrons escaping at about 42 deg from the incident beam path are directed toward the analyzer entrance. Because an additional accelerating field is necessary for the observation of onset differences, and because this field directionally narrows the emitted secondary electron distribution, a special sample stage was constructed at 45 deg to maximize the collection of secondary electrons. The sample is biased negatively, the grid and analyzer being grounded. The grid-to-sample distance used was typically 0.02 in., with 20 V of applied accelerating potential, giving a field of ~ 400 V/cm. A provision was also included to permit in-situ heating of samples up to approximately 1200°C. The final sample configuration used for the cathode studies is schematically represented in Fig. 2. The electronic hardware used for the signal acquisition and processing to produce the work-function maps is described in Reference 7.

⁷R. L. Corbin, Masters Thesis, California State University, Long Beach, Calif. (to be published).

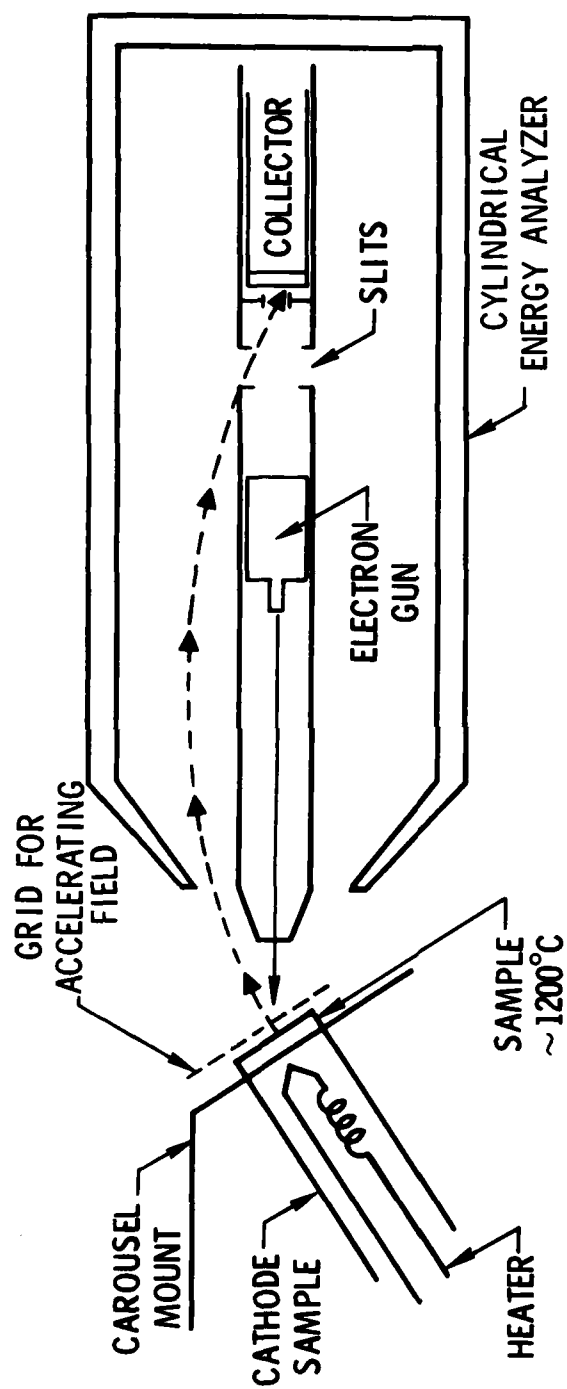


Fig. 2. Experimental Configuration, Revealing Cathode Sample, Biasing Grid, and Scanning Auger Microprobe Analyzer

IV. RESULTS AND DISCUSSION

A. RESULTS USING ELEMENT SAMPLES

Elemental niobium, platinum, and tungsten were examined to ascertain if their work-function differences could be measured by the onset of the secondary electron emission method. A sample consisting of 3-mil niobium wire co-wound with 1-mil platinum and 1-mil tungsten wires was cleaned in situ by a combination of heating and argon ion sputtering. Auger analysis of the wires indicated the presence of residual carbon, which is commonly observed on sputter-cleaned surfaces in vacuo. Also revealed was a significant amount of rhodium impurity in the platinum wire. The resultant onsets are presented in Fig. 3. The vertical scale is logarithmic in collected electron intensity and indicates an almost parallel shifted onset region for each of the three wires, with niobium being the lowest and platinum-rhodium the highest on the scale. The measured onset differences indicate that the platinum surface work function is contaminated by the relatively low work-function rhodium impurity, and the set of curves compares favorably with the published ϕ values, in eV, for elemental polycrystalline samples⁸

$$\phi(\text{Nb}) = 4.0, \phi(\text{W}) = 4.54, \phi(\text{Rh}) = 4.75, \phi(\text{Pt}) = 5.3$$

A second sample was prepared with niobium and platinum materials placed adjacent to each other to further test the mapping capability of this work-function method. This sample, which was fabricated by spot welding flattened niobium wire to a pure platinum foil, is illustrated in Fig. 4(a). Auger analysis after cleaning indicated again the presence of residual carbon and some oxygen on the niobium surface but no trace of rhodium in the platinum. The work-function maps contain large uniform ϕ patches, as would be expected from the flat sample geometry. Figures 4(b) and 4(c) reveal two ϕ maps, one

⁸V. S. Fomenko, Emission Properties of Materials, JPRS-56579, National Technical Information Service, Arlington, Virginia (1972).

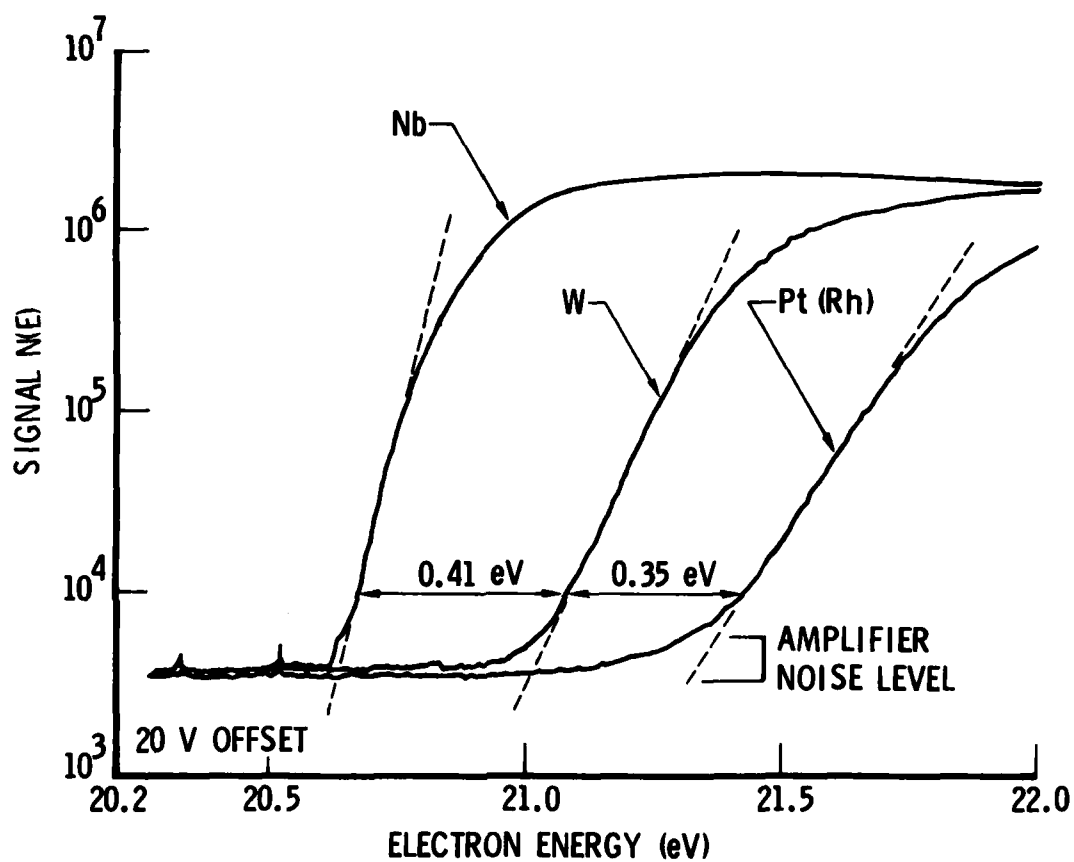


Fig. 3. Measured Shifts in Secondary Emission Onset Giving Work-Function Differences; Nb-W-Pt(Rh) Sample

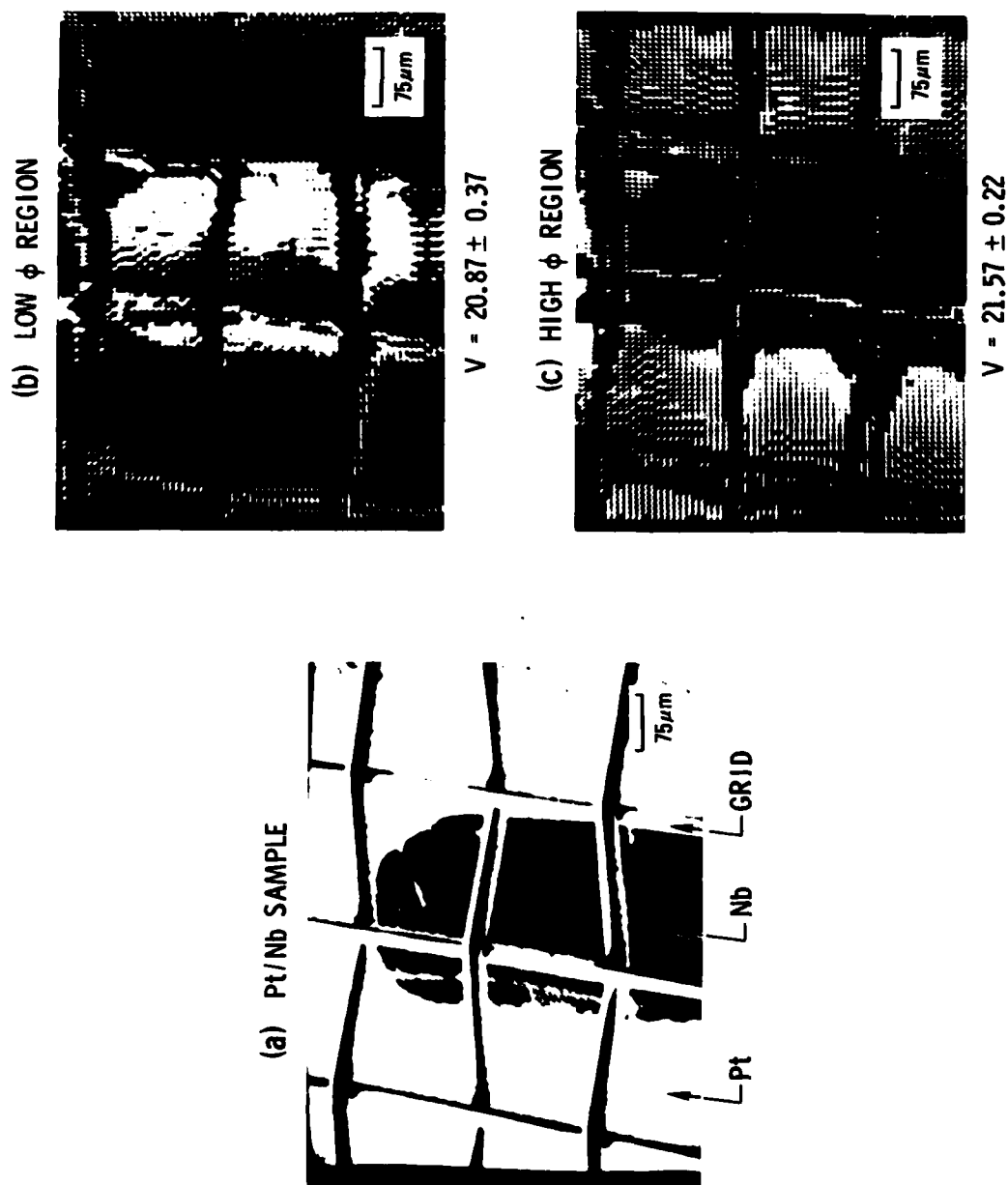


Fig. 4. Test of Work-Function (ϕ) Mapping with the Use of Pt/Nb Sample, Revealing Low ϕ Regions as Nb, High ϕ Regions as Pt. Grid for applying sample bias is also shown.

for the low work-function region ($V = 20.87 \pm 0.37$, 20-V offsets, $\Delta\phi = e\Delta V$), which covers the entire niobium region, and one for the high work-function region ($V = 21.57 \pm 0.22$), which covers the entire platinum region. Individual work-function maps taken at 0.2-eV intervals from $\phi(\text{minimum})$ to $\phi(\text{maximum})$ are presented in Fig. 5. Each of these maps was taken with a voltage band of ± 0.10 eV, so that the map labeled " $\phi(\text{min}) + 0.4$ eV" covers a band from $\phi(\text{minimum}) + 0.30$ eV to $\phi(\text{minimum}) + 0.5$ eV. These finer resolution ϕ maps can be used to obtain a surface work-function distribution $n(\phi)$ that represents the fraction of area within a given work-function range. This $n(\phi)$ is indicated in Fig. 6, normalized to account for the different relative niobium and platinum surface areas.

The uniformity of the individual ϕ maps over distances of approximately 100 μm and the two-dimensional spatial coherence that constitutes the ϕ -map image reveal the successful application of this ϕ technique in a mapping mode.

B. RESULTS ON COMMERCIAL DISPENSER CATHODES

After ϕ mapping was successfully demonstrated with the use of elemental samples, the technique was applied to examine the surfaces of commercial dispenser cathodes. The emphasis was on the use of the combined spatially resolved techniques of Auger analysis and work-function determination. Figure 7(a) reveals the surface of a dispenser cathode during the activation procedure, which involves heating and drawing current during the first 1 to 5 hr of cathode life. This procedure is standard practice when a cathode is first used in a device. During this period, surface barium appears. The Auger maps taken at approximately 800°C for barium and carbon are presented in Fig. 7(b). The barium map is bright where there is significant barium present and dark where there is less barium. The carbon map shown is a negative image, brighter where there is a lack of carbon and darker where there is more carbon. Three ϕ maps are shown in Fig. 7(c), one each for low, intermediate, and high ϕ values. Each of the lower work-function bands nests within the next higher ϕ map. Together, the maps reveal the entire low ϕ region to be

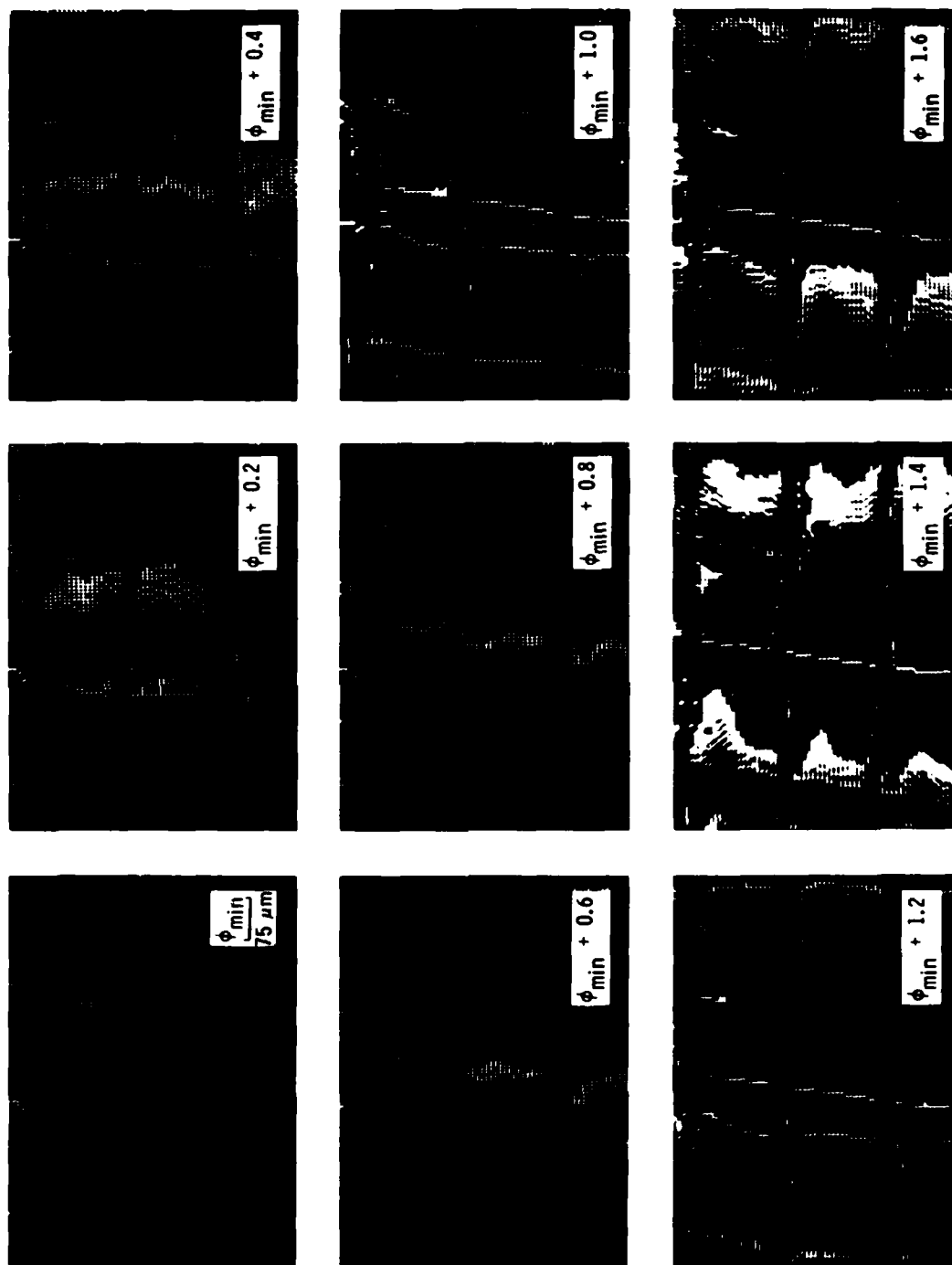


Fig. 5. Individual Work-Function Maps, Cleaned Pt/Nb Sample, 0.2-eV Intervals. Argon-ion sputtering gun used for in-situ cleaning would be at upper left. Some shadowing of sputtering ions by the grid is also evident.

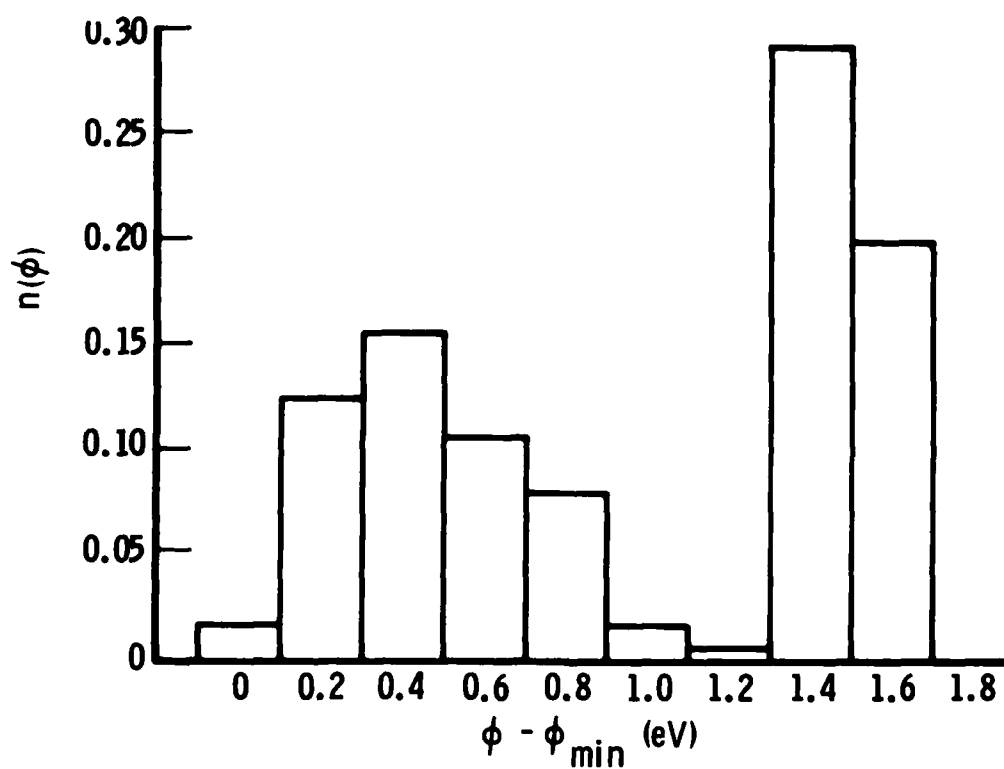


Fig. 6. Work-Function Distribution $n(\phi)$ Derived from Previous Figure, Normalized to Account for Differing Pt and Nb Surface Areas

CAPABILITIES:

SCANNING ELECTRON
MICROGRAPHS
FOR TOPOGRAPHICAL FEATURES



COMMERCIAL DISPENSER CATHODE

(a)

SCANNING AUGER
MICROGRAPHS
FOR ELEMENTAL CONCENTRATIONS



BARIUM
DISTRIBUTION
MAP



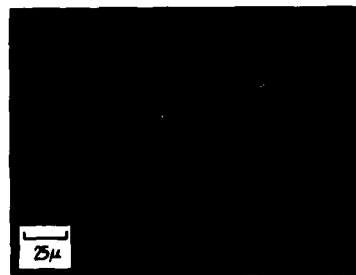
ANTI-
CARBON
DISTRIBUTION
MAP

(b)

SPATIALLY RESOLVED
WORK FUNCTION MAPS
FOR LOCAL ELECTRON EMISSIVITY



LOW
($\phi_{\min} + 0.25 \text{ eV}$)



INTERMEDIATE
($\phi_{\min} + 0.75 \text{ eV}$)

(c)



HIGHER-WORK FUNCTION
($\phi_{\min} + 1.25 \text{ eV}$)

Fig. 7. Example of Auger Elemental Distribution Taken on a Commercial Dispenser Cathode Surface During Activation Procedure ($\sim 800^\circ\text{C}$), Followed by Work-Function Maps (Room Temperature)

located where there is a significant amount of barium present. However, the lowest ϕ map indicates that the lowest ϕ area contains surface barium and lacks carbon.

As heating of the cathode surface continued during this early cathode life period (10 to 150 hr of heating at 1050°C), aggregates of approximately 0.3- μ m predominantly barium-oxide impregnant particles were found, often near pores and grain boundaries. Auger analyses also indicated that much of the exposed tungsten grains have an essentially uniform barium coverage. At these elevated temperatures, most of the surface carbon seen at lower temperatures has also been oxidized away. Figure 8 reveals these various cathode surface structures, at high magnification, after approximately 150 hr of heating near 1050°C. Even on this small scale, significant spatial inhomogeneity is evident. It also indicates that each of the three regions - impregnant filled pore ends, surface impregnant particles, and barium-oxygen covered tungsten - has a progressively higher work-function value.

C. COMPARISON OF SECONDARY ELECTRON ONSET TECHNIQUE WITH A RETARDING-BEAM METHOD

A direct comparison of the secondary electron onset technique with the retarding-beam method of Haas and Thomas⁴ was attempted. The retarding-beam method is also a spatially resolved technique but one in which an incident electron beam is reflected by a large applied decelerating field. Both the onset technique and the retarding-beam method rely on the fact that an inhomogeneous work-function surface will result in potential differences between given sample microregions and a grid held at a fixed potential.

The favored geometry for the onset technique is to have the sample normally inclined approximately at $\theta = 45$ deg from the beam direction to aim emitted secondary electrons toward the SAM cylindrical analyzer. But in order to be able to address the same spatial point by both methods, a $\theta = 0$ deg geometry must be used. However, it was found that in this geometry, many of the collected secondary electrons had been scattered at large angles from the direction of the surface normal. These secondaries have a greater chance of interacting with the grounded grid, releasing additional secondary electrons,

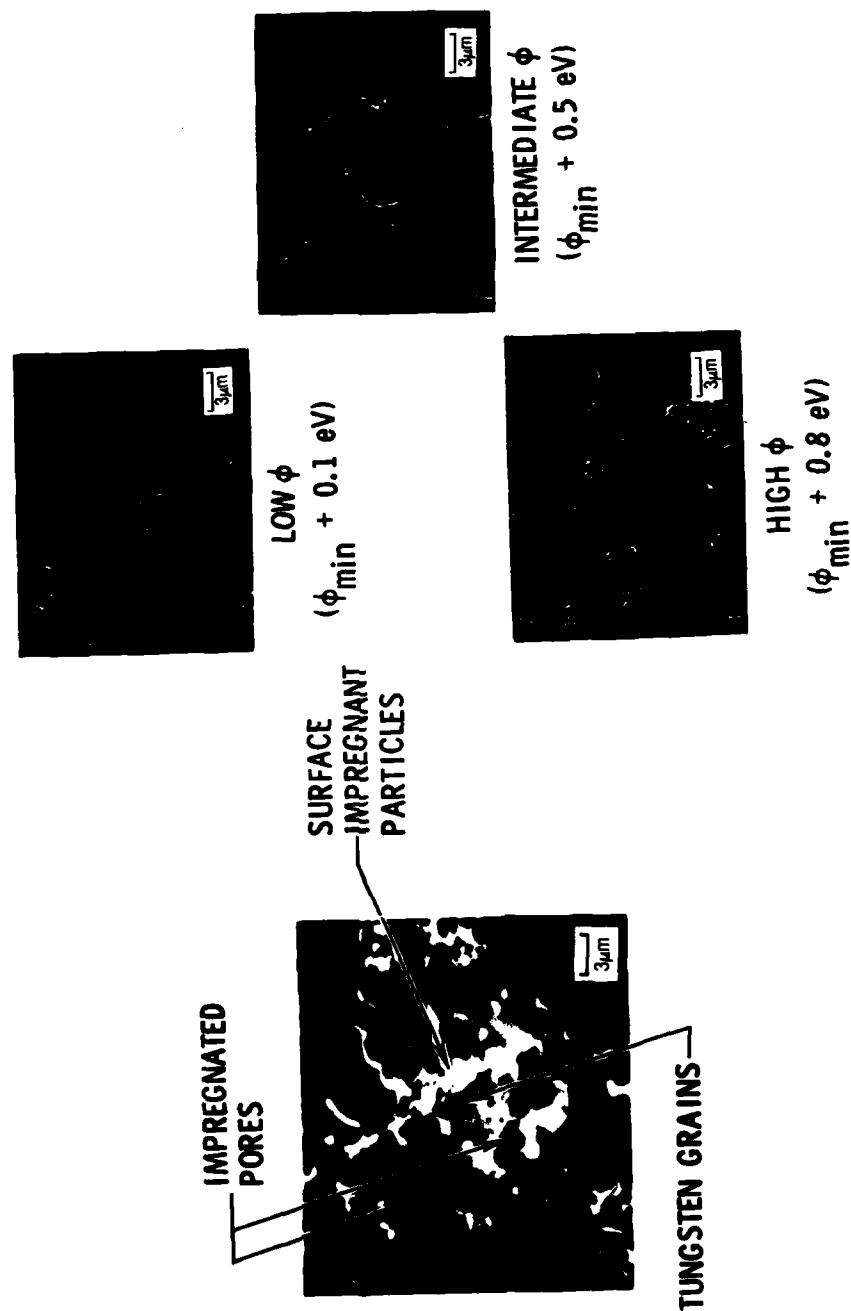


Fig. 8. Work-Function Maps Associated with a Cathode Microregion, after ~ 150 hr Heating at 1050°C , Revealing ϕ Correlation with Various Surface Features

which raises the background level significantly. Whereas a signal-to-background ratio exceeding 100 is obtained in the $\theta = 45$ deg configuration (see Fig. 3), it was reduced to as low as 2 for the $\theta = 0$ deg configuration. The apparent onset of secondary electron emission, under these conditions, can be far removed from the low-signal level required for a proper onset threshold measurement. A quantitative comparison of the two methods within our ϕ measurement system was thus precluded by incompatible geometrical requirements.

D. ACCURACY OF WORK-FUNCTION DETERMINATION

There are four potential sources of error in using the onset technique for the determination of work-function differences. They are: (1) beam induced charging of the sample, (2) errors introduced by patch fields and externally applied fields, (3) signal background overlapping the onset signal, and (4) finite resolution of the energy analyzer.

Charging on a dispenser cathode sample can possibly occur in regions of thick impregnant at low temperatures. However, sample charging characteristically manifests itself as random time-dependent energy shifting of the measured spectrum, and we have not seen indications of this in our samples. Conceivably, though, a resistive surface layer with negligible capacitance could introduce a stable shift in the secondary emission onset, skewing the work-function measurement. We have not yet investigated this possibility on dispenser cathode surfaces.

For samples where charging and resistive effects can be neglected, patch fields and externally applied electric fields can change the net potential barrier seen by an emitted electron, for both thermionic and secondary electrons. Any electron-beam technique actually monitors this net barrier height, thus giving rise to an inherent error Δw in the work function determination. An estimate for this error may be obtained by using:⁹

⁹G. A. Haas and R. E. Thomas, "Thermionic Emission and Work Function, " in Techniques of Metals Research, Vol. 6, Part 1, E. Passaglia, ed., Interscience, New York (1972).

$$eV(x) = -(\bar{\phi} - \phi_o) [1 - x(x^2 + 0.25D^2)^{-1/2}] - \phi_o [x_o/(x + x_o)] - eE_o x$$

$$x_o \equiv e^2/(4\pi\epsilon_o \phi_o)$$

in which the potential $V(x)$ is described at a distance x above the center of a circular patch of diameter D in the presence of an applied field E_o . The true patch work function is ϕ_o , and the patch is surrounded by an area whose average work function is $\bar{\phi}$; accelerating field conditions ($E_o > 0$) are assumed. The maximum of this function determines x^* , an effective barrier width, and $eV(x^*)$, an effective barrier height, from which Δw can be estimated:

$$\Delta w = (\bar{\phi} - \phi_o) \{x^*/[(x^*)^2 + 0.25D^2]^{1/2}\} - \phi_o [x_o/(x^* + x_o)] - eE_o x^*$$

This Δw represents the minimum error associated with the work-function measurement, because it is determined from immediately above the patch center. Contributions from off-center points may produce a larger error. For Δw positive, the measured apparent work function is higher than the true value; for Δw negative, it is lower than true value. The measured work-function value for the patch $\phi(\text{meas})$, is the sum of $\bar{\phi}$ and $eV(x^*)$. Figure 9(a) reveals the error in $\phi(\text{meas})$, Δw , plotted against patch size D , for patches that differ ± 1.00 eV from the average value $\bar{\phi}$, using $E_o = 400$ V/cm. Using families of curves similar to Fig. 9(a), the regions of acceptable patch size D versus measured work-function difference $\Delta\phi \equiv \bar{\phi} - \phi(\text{meas})$ can be constructed. This is shown in Fig. 9(b), which is divided into two regions: region I, the area above the plotted curve, in which the error in work-function determination Δw is less than ± 0.05 eV; and region II, the remaining area, in which Δw is greater than ± 0.05 eV. This plot can be used to determine the accuracy of the work-function measurement. For example, patches $4.0 \mu\text{m}$ or larger can differ from 0.0 to 1.0 eV below the surface average $\bar{\phi}$ and still be within the 0.05-eV error bounds. But patches of $1.0 \mu\text{m}$ are permitted only to differ from 0.0 to 0.3 eV below the surface average value, before the 0.05-eV error point is reached.

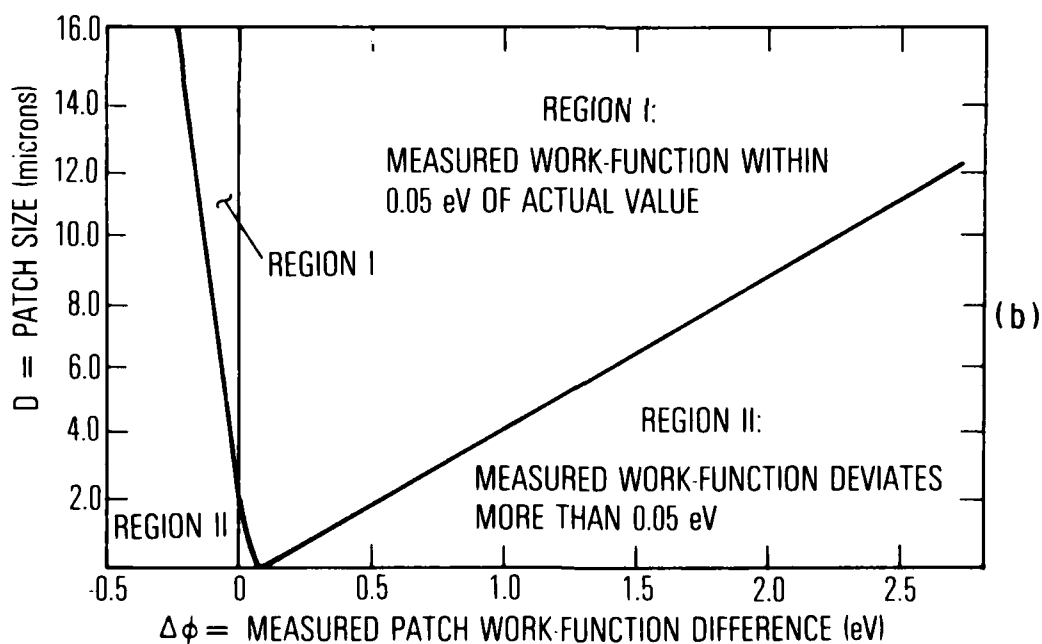
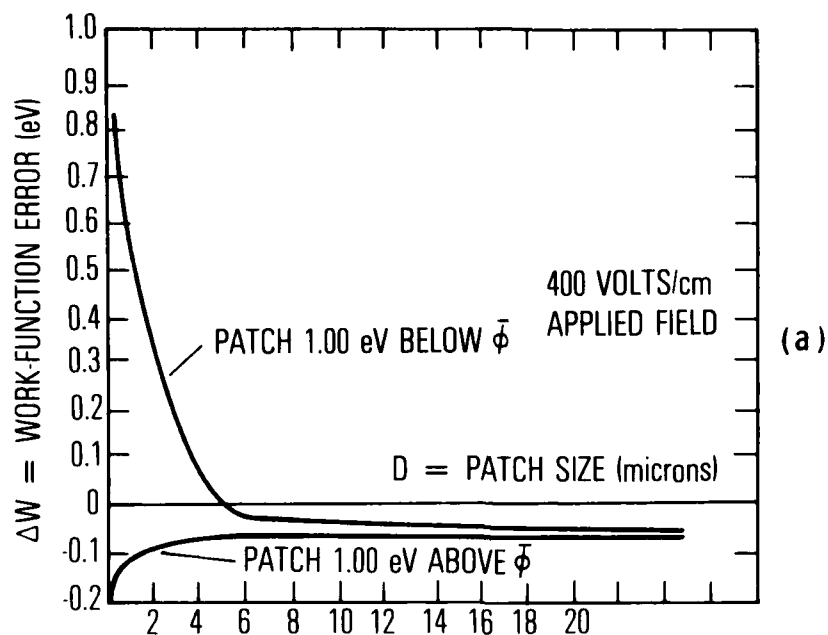


Fig 9. Calculated Effects of Patch Fields on Work-Function Measurement. Upper curves show error in work-function determination (Δw , eV) vs. patch size (D , microns). Lower curve shows range of allowable patch size vs. measured work-function difference from surface average value $\bar{\phi}$ at 400 V/cm applied field.

Signal background presents an error, because the background can obscure the true onset region in the collected $N(E)$ signal versus energy spectrum. More accurate $\Delta\phi$ values may be derived from this onset technique by extrapolating to zero-signal level, instead of using an arbitrarily set low-level threshold. This is essentially a background subtraction procedure that can correct for the sloping rise in the collected signal intensity (see Fig. 3), and it is about a 0.03-eV correction.

Finally, the cylindrical energy analyzer has a finite resolution, $\Delta E/E \sim 0.3\%$, which introduces a systematic convolution into the measured signal. For an offset voltage of ~ 20 V, this gives a $\Delta E \sim 0.06$ eV, but its main effect should be to give a sloping rise output if given a step jump in actual signal. Much of this effect is subtracted away in a work-function difference measurement.

V. CONCLUSIONS

The capability for performing high-resolution, spatially resolved work-function measurements has been demonstrated using the variation in secondary electron emission onsets. It has been successfully implemented in a scanning mode and integrated into a scanning auger microprobe (SAM) facility. The combined system permits both work-function maps and a correlation of emissive properties and chemical composition within any given surface microregion. It has a spatial resolution determined primarily by beam diameter, and a work-function resolution of better than 0.05 eV, limited primarily by a trade-off of patch-size and work-function deviation from the surrounding. As part of a combined SAM spatially resolved work-function system, it easily provides concurrent Auger and ϕ mapping of surface features of size $\sim 4.0 \mu\text{m}$ or larger.

Because this ϕ measurement method relies on the onset of the secondary electron spectrum, it is, in general, compatible with electron microprobe systems, and the resultant $\Delta\phi$ measurements are in good agreement with literature values.

LABORATORY OPERATIONS

The Laboratory Operations of The Aerospace Corporation is conducting experimental and theoretical investigations necessary for the evaluation and application of scientific advances to new military concepts and systems. Versatility and flexibility have been developed to a high degree by the laboratory personnel in dealing with the many problems encountered in the Nation's rapidly developing space systems. Expertise in the latest scientific developments is vital to the accomplishment of tasks related to these problems. The laboratories that contribute to this research are:

Aerophysics Laboratory: Aerodynamics; fluid dynamics; plasmadynamics; chemical kinetics; engineering mechanics; flight dynamics; heat transfer; high-power gas lasers, continuous and pulsed, IR, visible, UV; laser physics; laser resonator optics; laser effects and countermeasures.

Chemistry and Physics Laboratory: Atmospheric reactions and optical backgrounds; radiative transfer and atmospheric transmission; thermal and state-specific reaction rates in rocket plumes; chemical thermodynamics and propulsion chemistry; laser isotope separation; chemistry and physics of particles; space environmental and contamination effects on spacecraft materials; lubrication; surface chemistry of insulators and conductors; cathode materials; sensor materials and sensor optics; applied laser spectroscopy; atomic frequency standards; pollution and toxic materials monitoring.

Electronics Research Laboratory: Electromagnetic theory and propagation phenomena; microwave and semiconductor devices and integrated circuits; quantum electronics, lasers, and electro-optics; communication sciences, applied electronics, superconducting and electronic device physics; millimeter-wave and far-infrared technology.

Materials Sciences Laboratory: Development of new materials; composite materials; graphite and ceramics; polymeric materials; weapons effects and hardened materials; materials for electronic devices; dimensionally stable materials; chemical and structural analyses; stress corrosion; fatigue of metals.

Space Sciences Laboratory: Atmospheric and ionospheric physics, radiation from the atmosphere, density and composition of the atmosphere, aurorae and airglow; magnetospheric physics, cosmic rays, generation and propagation of plasma waves in the magnetosphere; solar physics, x-ray astronomy; the effects of nuclear explosions, magnetic storms, and solar activity on the earth's atmosphere, ionosphere, and magnetosphere; the effects of optical, electromagnetic, and particulate radiations in space on space systems.